Properties of Human Serum Albumin Entrapped in Sol−Gel-Derived Silica Bearing Covalently Tethered Sugars

Xihua Sui, Jorge A. Cruz-Aguado, Yang Chen, Zheng Zhang, Michael A. Brook, and John D. Brennan*

Department of Chemistry, McMaster University, 1280 Main Street West, Hamilton, Ontario L8S 4M1, Canada

Received October 18, 2004. Revised Manuscript Received January 10, 2005

Silica derived from biocompatible silane precursors and containing covalently bound sugar moieties has recently been reported to be a much more biocompatible matrix for protein entrapment than any previously synthesized materials. To better understand the nature of these new materials, the steady-state and time-resolved fluorescence of human serum albumin (HSA) was used to examine the conformation, dynamics, accessibility, thermal stability, and degree of ligand binding after entrapment of the protein into sol−gel-processed glasses derived from either tetraethyl orthosilicate (TEOS) or diglycerylsilane (DGS), which in some cases contained covalently bound gluconamidylsilane (GLS) moieties. It was observed that the initial conformation, accessibility to external analytes, thermal stability, long-term stability, and degree of ligand binding to HSA were best in DGS-derived materials that contained covalently tethered GLS relative to unmodified DGS-derived materials, TEOS, or TEOS/GLS-derived materials. Measurement of protein rotational dynamics showed that entrapment led to an immediate loss of global motion in all materials. However, the restriction of motion was most dramatic in GLS-doped materials, suggesting preferential interactions of the protein with the sugar-coated surfaces. As aging proceeded, both protein dynamics and the degree of ligand binding decreased, with a gradual loss of segmental motion and a significant increase in local motion in the vicinity of the probe, consistent with unfolding and surface adsorption of the protein, leading to loss of function. Overall, our findings suggest that the use of a biocompatible precursor (DGS) and the addition of a covalently bound sugar both contribute to improved protein performance. However, of these two the use of a biocompatible precursor is the most important factor, and in such cases addition of sugars further improves protein performance. In contrast, the use of the sugar-based additive with a nonbiocompatible precursor such as TEOS imparted essentially no benefit, demonstrating the importance of biocompatible processing conditions.

Introduction

An emerging method for immobilization of proteins is their entrapment into a porous, inorganic silicate matrix that is formed via a low-temperature sol−gel-processing method.[1,2] Numerous reports have described both fundamental aspects of entrapped proteins, such as their conformation,[3−5] dynamics,[6−8] accessibility,[5,9] reaction kinetics,[3,10] activity,[11−21] and stability,[22−29] and their many applications for catalysis, sensing, and affinity chromatography.[1,2] From these studies

* To whom correspondence should be addressed. Phone: (905) 525-9140 (ext. 27033). Fax: (905) 527-9950. E-mail: brennanj@mcmaster.ca. Web page: http://www.chemistry.mcmaster.ca/faculty/brennan.

(1) Gill, I. *Chem. Mater*. **2001**, *13*, 3404−3421.
(2) Jin, W.; Brennan, J. D. *Anal. Chim. Acta* **2002**, *461*, 1−36.
(3) Zheng, L.; Reid, W. R.; Brennan, J. D. *Anal. Chem*. **1997**, *69*, 3940−3949.
(4) Zheng, L.; Brennan, J. D. *Analyst* **1998**, *123*, 1735−1744.
(5) Edmiston, P. L.; Wambolt, C. L.; Smith, M. K.; Saavedra, S. S. *J. Colloid Interface Sci*. **1994**, *163*, 395−406.
(6) Jordan, J. D.; Dunbar, R. A.; Bright, F. V. *Anal. Chem*. **1995**, *67*, 2436−2443.
(7) Gottfried, D. S.; Kagan, A.; Hoffman, B. M.; Friedman, J. M. *J. Phys. Chem. B* **1999**, *103*, 2803−2807.
(8) Doody, M. A.; Baker, G. A.; Pandey, S.; Bright, F. V. *Chem. Mater*. **2000**, *12*, 1142−1147.
(9) Wambolt, C. L.; Saavedra, S. S. *J. Sol-Gel Sci. Technol*. **1996**, *7*, 53−57.
(10) Shen, C.; Kostic, N. M. *J. Am. Chem. Soc*. **1997**, *119*, 1304−1312.
(11) Braun, S.; Shtelzer, S.; Rappoport, S.; Avnir, D.; Ottolenghi, M. *J. Non-Cryst. Solids* **1992**, *147*, 739−743.
(12) Avnir, D.; Braun, S.; Lev, O.; Ottolenghi, M. *Chem. Mater*. **1994**, *6*, 1605−1614.
(13) Wang, R.; Narang, U.; Prasad, P. N.; Bright, F. V. *Anal. Chem*. **1993**, *65*, 2671−2675.
(14) Ellerby, L. M.; Nishida, C. R.; Nishida, F.; Yamanaka, S. A.; Dunn, B.; Valentine, J. S.; Zink, J. I. *Science* **1992**, *225*, 1113−1115.
(15) Wu, S.; Ellerby, L. M.; Cohan, J. S.; Dunn, B.; El-Sayed, M. A.; Valentine, J. S.; Zink, J. I. *Chem. Mater*. **1993**, *5*, 115−120.
(16) Dave, B. C.; Soyez, H.; Miller, J. M.; Dunn, B.; Valentine, J. S.; Zink, J. I. *Chem. Mater*. **1995**, *7*, 1431−1434.
(17) Yamanaka, S. A.; Nishida, F.; Ellerby, L. M.; Nishida, C. R.; Dunn, B.; Valentine, J. S.; Zink, J. I. *Chem. Mater*. **1992,** *4*, 495−497.
(18) Dave, B. C.; Dunn, B.; Valentine, J. S.; Zink, J. I. *Anal. Chem*. **1994**, *66*, 1120A−1127A.
(19) Blyth, D. J.; Aylott, J. W.; Richardson, D. J.; Russell, D. A. *Analyst* **1995**, *120*, 2725−2730.
(20) Aylott, J. W.; Richardson, D. J.; Russell, D. A. *Analyst* **1997**, *122*, 77−80.
(21) Williams, A. K.; Hupp, J. T. *J. Am. Chem. Soc*. **1998**, *120*, 4366−4371.
(22) Braun, S.; Rappoport, S.; Zusman, R.; Avnir, D.; Ottolenghi, M. *Mater. Lett*. **1990**, *10*, 1−5.
(23) Heichal-Segal, O.; Rappoport, S.; Braun, S. *Biotechnology* **1995**, *13*, 798−800.
(24) Reetz, M. T.; Zonta, A.; Simpelkamp, J. *Biotechnol. Bioeng*. **1996**, *49*, 527−534.
(25) Narang, U.; Prasad, P. N.; Bright, F. V.; Kumar, K.; Kumar, N. D.; Malhotra, B. D.; Kamalasanan, M. N.; Chandra, S. *Chem. Mater*. **1994**, *6*, 1596−1598.

10.1021/cm048166c CCC: $30.25
Published on Web 02/11/2005

it has become clear that processing methods that involve either low pH or high alcohol levels can destabilize proteins, causing a substantial loss of biological function upon entrapment,[30] and can cause significant structural changes in proteins immediately upon entrapment and as the materials age.[31]

In recent years, a number of sol−gel-derived materials have been designed with the purpose of making the matrix more compatible with entrapped biological molecules. For example, new biocompatible silane precursors and processing methods have recently been reported based on glycerated silanes,[1,32,33] sodium silicate,[34] or aqueous processing methods that involve removal of alcohol byproducts by evaporation before the addition of proteins.[35] Other approaches to improve protein stability, including the use of protein-stabilizing additives such organosilanes,[29,36−38] polymers,[39−43] or sugars and amino acids (osmolytes)[44,45] to silica, have also been reported.

Recently, our group reported two advances in the development of sol−gel-processed materials: (1) the development of new sol−gel precursors, such as diglycerylsilane (DGS), that release protein-stabilizing compounds upon hydrolysis[32,46] and (2) the preparation of silica precursors bearing covalently bound sugars, such as gluconamidylsilane (GLS),[47] which result in the formation of sugar-modified silica materials. Together, these compounds have been shown to produce materials that are amenable to entrapment of a number of delicate proteins, including urease, factor Xa, Src kinase, and luciferase, none of which remain active upon entrapment into silica materials derived from conventional alkoxysilanes.

While sugar-modified silica materials have been demonstrated to be suitable hosts for many enzymes, little has been done to characterize the roles that either the DGS precursor or the GLS additive plays in controlling protein activity. The utility of an entrapped protein is determined primarily by its ability to retain a native conformation after entrapment and remain accessible to external analytes that enter the matrix. In addition, the protein should be sufficiently mobile to be able to undergo any necessary conformational changes upon binding of analyte to produce a desired reaction or signal.[2]

In this work, we have monitored the behavior of the model protein human serum albumin (HSA) as a function of time after entrapment into silica materials derived from either tetraethyl orthosilicate (TEOS) or DGS, with or without covalently bound GLS. HSA was chosen because it is relatively large and complex (MW of 66000 with three major domains) but yet contains only a single Trp residue within the protein at position 214 in domain II and a single cysteine at position 34 in domain I which is suitable for site-selective labeling, allowing for a detailed fluorescence analysis of protein conformation and dynamics. HSA was also chosen because its behavior has been well characterized both in solution[48] and in TEOS-derived materials,[31] allowing comparisons with previous studies. In the present work, the steady-state and time-resolved fluorescence of unlabeled and labeled HSA was used to provide information on the conformation, thermal stability, long-term stability, analyte accessibility, protein dynamics, and ligand-binding properties of HSA entrapped in the silica materials described above. These parameters were used to provide an overall picture of the properties of HSA when entrapped in various silica materials, and provide clear insights into the role that both the biocompatible precursor and the covalently bound sugar play in maintaining the activity of entrapped proteins.

Experimental Section

Chemicals. DGS[32,46] and *N*-(3-triethoxysilylpropyl)gluconamide (GLS)[47,49,50] were prepared by methods described elsewhere. Human serum albumin, salicylic acid, and polymethacrylate fluorimeter cuvettes were obtained from Sigma. Fluorescein-5-maleimide was obtained from Invitrogen (Oakville, ON). TEOS (99.999+%), cobalt chloride (99.9%), and potassium iodide (99.9%) were purchased from Anachemia. All water was distilled and deionized on a Milli-Q

(26) Narang, U.; Prasad, P. N.; Bright, F. V.; Ramanathan, K.; Kumar, N. D.; Malhotra, B. D.; Kamalasanan, M. N.; Chandra, S. *Anal. Chem.* **1994**, *66*, 3139−3144.
(27) Jordan, J. D.; Dunbar, R. A.; Bright, F. V. *Anal. Chim. Acta* **1996**, *332*, 83−91.
(28) Yamanaka, S. A.; Dunn, B.; Valentine, J. S.; Zink, J. I. *J. Am. Chem. Soc.* **1995**, *117*, 9095−9096.
(29) Kauffmann, C.; Mandelbaum, R. T. *J. Biotechnol.* **1998**, *62*, 169−176.
(30) (a) Miller, J. M.; Dunn, B.; Valentine, J. S.; Zink, J. I. *J. Non-Cryst. Solids* **1996**, *220*, 279−289. (b) Dave, B. C.; Miller, J. M.; Dunn, B.; Valentine, J. S.; Zink, J. I. *J. Sol-Gel Sci. Technol.* **1997**, *8*, 629−634.
(31) Flora, K. K.; Brennan, J. D. *Chem. Mater.* **2001**, *13*, 4170−4179.
(32) (a) Brook, M. A.; Chen, Y.; Guo, K.; Zhang, Z.; Jin, W.; Deisingh, A.; Brennan, J. D. *J. Sol-Gel Sci. Technol.* **2004**, *31*, 343−348. (b) Brook, M. A.; Chen, Y.; Guo, K.; Zhang, Z.; Brennan, J. D. *J. Mater. Chem.* **2004**, *14*, 1469−1479.
(33) Gill, I.; Ballesteros, A. *J. Am. Chem. Soc.* **1998**, *120*, 8587−8598.
(34) Bhatia, R. B.; Brinker, C. J.; Gupta, A. K.; Singh, A. K. *Chem. Mater.* **2000**, *12*, 2434−2441.
(35) Ferrer, M. L.; del Monte, F.; Levy, D. *Chem. Mater.* **2002**, *14*, 3619−3621.
(36) Reetz, M. T.; Zonta, A.; Simpelkamp, J.; Konen, W. *Chem. Commun.* **1996**, 1397−1398.
(37) Reetz, M. T.; Zonta, A.; Simpelkamp, J. *Angew. Chem., Int. Ed. Engl.* **1995**, *34*, 301−303.
(38) Kuncova, G.; Guglielmi, M.; Dubina, P.; Safar, B. *Collect. Czech. Chem. Commun.* **1995**, *60*, 1573−1577.
(39) Altstein, M.; Segev, G.; Aharonson, N.; Ben-Aziz, O.; Turniansky, A.; Avnir, D. *J. Agric. Food Chem.* **1998**, *46*, 3318−3324.
(40) Wang, B. Q.; Li, B.; Deng, Q.; Dong, S. J. *Anal. Chem.* **1998**, *70*, 3170−3174.
(41) Wang, B. Q.; Dong, S. J. *Talanta* **2000**, *51*, 565−572.
(42) Zhang, J. Z.; Li, B.; Wang, Z.-X.; Cheng, G. J.; Dong, S. J. *Anal. Chim. Acta* **1999**, *388*, 71−78.
(43) (a) Chen, Q. Kenausis, G. L.; Heller, A. *J. Am. Chem. Soc.* **1998**, *120*, 4582−4585; b) Heller, J.; Heller, A. *J. Am. Chem. Soc.* **1998**, *120*, 4586−4590.
(44) Eggers, D. K.; Valentine, J. S. *J. Mol. Biol.* **2001**, *314*, 911−922.
(45) Brennan, J. D.; Benjamin, D.; Dibattista, E.; Gulcev. M. D. *Chem. Mater.* **2003**, *15*, 737−745.
(46) Besanger, T. R.; Chen, Y.; Deisingh, A. K.; Hodgson, R.; Jin, W.; Stanislas, M.; Brook, M. A.; Brennan, J. D. *Anal. Chem.* **2003**, *75*, 2382−2391.
(47) (a) Cruz-Aguado, J. A.; Chen, Y.; Zhang, Z.; Elowe, N.; Brook, M. A.; Brennan, J. D. *J. Am. Chem. Soc.* **2004**, *126*, 6878−6879. (b) Cruz-Aguado, J. A.; Chen, Y.; Brook, M. A.; Brennan, J. D. *Anal. Chem.* **2004**, *76*, 4182−4188.
(48) Flora, K. K.; Brennan, J. D.; Baker, G. A.; Doody, M. A.; Bright, F. V. *Biophys. J.* **1998**, *75*, 1084−1096.
(49) Tleugabulova, D.; Zhang, Z.; Chen, Y.; Brook, M. A.; Brennan, J. D. *Langmuir* **2004**, *20*, 848−854.
(50) Zhang, Z.; Chen, D. Y.; Brennan, J. D.; Brook, M. A. Methods and Compounds for Controlling the Morphology and Shrinkage of Silica Derived From Polyol-Modified Silanes. PCT/CA03/01257, filed Aug 23, 2003.

Synthesis A10 water purification system. All reagents were used without further purification.

Procedures. *Labeling of HSA.* Labeling of HSA at cysteine-34 using fluorescein-5-maleimide was done according to standard procedures.[48] Briefly, HSA was combined with a 25-fold molar excess of fluorescein-5-maleimide in a buffer system consisting of 20 mM Tris buffer containing 100 mM NaCl and 5 mM EDTA and reacted for 2 h in the dark. The labeled protein was then purified by size-exclusion chromatography using a Sephadex G-25 column. The concentration of labeled protein was found using $\epsilon_{473} = 83000$ M^{-1} cm^{-1} for fluorescein (dianion),[51] and $\epsilon_{277} = 36000$ M^{-1} cm^{-1} for HSA.[52] The labeling efficiency was determined to be ~25%.

Entrapment of Protein. HSA was diluted into Tris-buffered saline solution (50 mM Tris, 150 mM NaCl, 5 mM EDTA) to a concentration of 10 μM, as determined using UV/vis absorbance measurements. The DGS sol was prepared by adding 0.4 g of solid DGS to 1 mL of distilled water followed by sonication in an ice bath for 1 h, after which the DGS solution was filtered using a 0.45 μm Acrodisc syringe filter (Pall Corp., Ann Arbor, MI) to remove any solid particulates. TEOS sols were prepared by sonicating a mixture of 4.5 mL of TEOS, 1.4 mL of water, and 100 μL of 0.1 N HCl for 1 h at ambient temperature until the mixture became clear, colorless, and monophasic. GLS solutions were prepared by dissolving 0.15 g of GLS into 1 mL of Tris-buffered saline solution. Sol mixtures without GLS were prepared in the form of monolithic blocks (1.5 cm × 1 cm × 1 cm) by mixing 0.75 mL of the DGS- or TEOS-derived sol with 0.75 mL of the protein solution. Sol mixtures with GLS were prepared by mixing 0.75 mL of the sol with 0.75 mL of the protein solution, which contained a sufficient amount of GLS to result in a 17 mol % ratio of GLS to silica. This level of GLS was selected on the basis of previous work that indicated optimal enzyme performance at levels of 15−20 mol % GLS.[47] All samples were aged in air for varying amounts of time (see below) at 4 °C prior to testing.

Steady-State Fluorescence Measurements. Fluorescence measurements were performed using an SLM 8100 spectrofluorimeter (Spectronic Instruments, Rochester, NY) as described elsewhere.[3] Intrinsic tryptophan emission spectra of HSA were collected from 305 to 450 nm with excitation at 295 nm. All spectra were collected in 1 nm increments using 8 nm band-passes on the excitation and emission monochromators and an integration time of 0.3 s per point. Appropriate blanks were subtracted, and the resulting spectra were corrected for the wavelength dependence of the emission monochromator and PMT.

Steady-state fluorescence anisotropy measurements were performed in the L format using Glan-Taylor prism polarizers in the excitation and emission paths, as described previously.[3,4] Single-point fluorescence anisotropy measurements were generally made at the maximum emission wavelength, using excitation at 295 nm for Trp or 495 nm for fluorescein. Band-passes of 8 nm were used in the excitation and emission paths, with the signal integrated for 3 s. Appropriate blanks were subtracted from each of the intensity values (I_{VV}, I_{VH}, I_{HV}, I_{HH}) used to calculate the anisotropy values, and all fluorescence anisotropy values were corrected for the instrumental G factor to account for any polarization bias in the monochromators. The values reported represent the average of five measurements each on three samples.

Time-Resolved Fluorescence. Time-resolved fluorescence intensity and anisotropy decay data of fluorescein-labeled HSA were acquired in the time domain using an IBH 5000U time-correlated single-photon-counting fluorimeter, as described elsewhere.[49] Time-resolved decays of fluorescence anisotropy were constructed from intensity decays that were obtained using vertically polarized excitation and vertically polarized emission (I_{VV}) or horizontally polarized emission (I_{VH}) and were corrected for the instrument response profile and the instrumental G factor. The anisotropy decay was fit to a two-component hindered rotor model according to the following equation:[53]

$$r(t) = f_1 r_0 \exp(-t/\phi_1) + f_2 r_0 \exp(-t/\phi_2) + g r_0 \qquad (1)$$

where ϕ_1 reflects rapid rotational motions associated with rotation of bound fluorescein in the region of Cys-34, ϕ_2 reflects slower reorientation associated with global or segmental motion of the protein, f_1 is the fraction of fluorescence associated with ϕ_1, f_2 is the fraction of fluorescence associated with ϕ_2, g is the fraction of fluorescence due to probes that rotate more slowly than can be measured with the fluorescein probe (ϕ > 60 ns), and r_0 is the limiting anisotropy. In some cases, the value of gr_0 is denoted as r_∞, which is the residual anisotropy of the protein owing to hindered global rotation. Fits were considered acceptable if the reduced χ^2 (χ_R^2) was close to 1.0 and the residuals showed no clearly nonrandom pattern.

Thermal Stability Studies. Fluorescence-based thermal denaturation studies of entrapped HSA were done as described previously.[4,31] Samples were degassed using nitrogen prior to thermal denaturation to reduce the potential for oxidation of the Trp residue at high temperatures. The integrated emission intensity of Trp-214 was plotted against sample temperature, and the midpoint of the resulting unfolding curve was determined by nonlinear fitting to extract unfolding temperatures (T_{un}). An equilibration time of 30 min was allowed at each temperature before emission spectra were collected. This equilibration time was found to be sufficient, as the signal did not change when using longer equilibration times. Cooling the samples indicated that the unfolding transition was not reversible (in agreement with studies of HSA denaturation in solution[48]); thus, thermodynamic parameters related to the protein unfolding event could not be obtained.

Quenching Studies. Iodide and cobalt quenching studies were done for HSA in solution and in DGS- and TEOS-derived monoliths with and without GLS present, respectively. For solution studies, a 30 μM HSA solution was titrated by adding varying aliquots of 6.0 M potassium iodide or 3.5 M cobalt chloride in buffer with continuous stirring. Spectra were corrected for sample dilution and were integrated to obtain fluorescence intensity values. For studies of entrapped HSA, the dimensions of the blocks were such that titrations required several hours per point to complete, owing to the very slow rate of diffusion of the quencher through the matrix. For this reason, individual monolithic samples (1.5 cm × 1 cm × 1 cm) that were formed at the same time and aged identically were incubated for 24 h with varying concentrations of potassium iodide or cobalt chloride in Tris buffer. A Trp fluorescence spectrum was collected from each sample and an appropriate blank, and the spectra were integrated to obtain fluorescence intensity values. The data from monoliths incubated with different quencher concentrations were combined to yield quenching curves. All quenching data were analyzed using the following equation:[31]

$$\frac{F_0(1 - f_i)}{F - f_i F_0} = 1 + K_{SV}[Q] = 1 + k_q \tau_0 [Q] \qquad (2)$$

where F_0 is the fluorescence intensity in the absence of the quencher, F is the fluorescence intensity at a given molar

(51) Sjöback, R.; Nygren, J.; Kubista, M. *Spectrochim. Acta, A* **1995**, *51A*, L7-L21.
(52) Pico, G. A. *Int. J. Biol. Macromol.* **1997**, *20*, 63−73.
(53) Geddes, C. D.; Karolin, J.; Birch, D. J. S. *J. Phys. Chem. B* **2002**, *106*, 3835-.

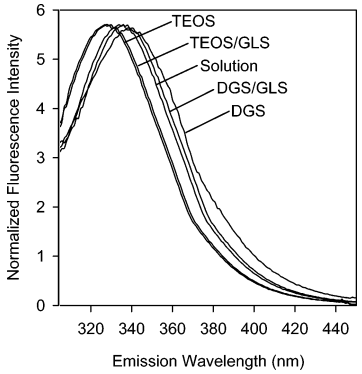

Figure 1. Emission spectra of HSA in solution and entrapped in different silica materials.

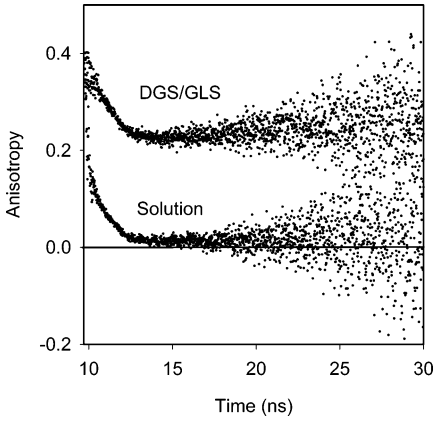

Figure 2. Time-resolved anisotropy decay curves for HSA in solution and entrapped in DGS/GLS-derived silica.

concentration of quencher [Q], f_i is the fraction of HSA which is inaccessible to quencher, K_{SV} is the Stern−Volmer quenching constant (M^{-1}), k_q is the bimolecular quenching rate constant (M^{-1} s^{-1}), and τ_0 is the unquenched fluorescence lifetime (s).

Salicylate Titrations of HSA. For studies of salicylate binding to entrapped HSA, individual monolithic samples (1.5 cm × 1 cm × 1 cm) containing 10 μM HSA were formed at the same time and aged identically, as above. The samples were incubated for 24 h with varying concentrations of salicylate in Tris buffer. A Trp fluorescence spectrum was collected from each sample and an appropriate blank. The intensity at 335 nm was plotted against salicylate concentration to yield binding curves. Dissociation constants were estimated by determining the amount of ligand that was required to reach 50% of the maximum change in the signal upon addition of salicylate to HSA. For time-dependent binding studies of free and entrapped HSA, measurements were done only at a 1.75:1 molar ratio of salicylate to protein, which was close to the level required to obtain maximum binding of the ligand by HSA in solution. The overall change in intensity was normalized to the change obtained in solution to estimate the extent of ligand binding to HSA.

Shrinkage and Pore Size Analysis. Shrinkage measurements were performed on samples that were aged in air for 60 days. Samples were prepared as blocks with initial dimensions of 1 cm × 1 cm × 2 cm. The volume of the materials after aging was determined by measurement of the shrunken blocks, and shrinkage values are reported relative to the original volume of the block. Pore-size analysis of completely dried monoliths was performed on a Quantachrome Nova 2000 surface area/pore size analyzer. Before analysis, the monoliths were washed copiously to remove any entrapped glycerol, crushed to a fine powder, freeze-dried, and outgassed at 120 °C for 4 h to remove air and bound water from the surface of the powder. The pressure was measured as nitrogen was adsorbed and desorbed at a constant temperature of −196 °C. Using the desorption branch of the resulting isotherm, the average pore size and distribution of pore sizes were determined using the BJH (Barrett, Joyner, and Halenda) calculation.[54] All data reported are the average of two measurements on different samples.

Results and Discussion

Steady-State Fluorescence Measurements of Entrapped HSA. Figure 1 shows the emission spectra of HSA in solution and 1 day after entrapment into different silica materials. For HSA in solution, the emission maximum was 335 nm, indicative of HSA in a native conformation.[31] Upon entrapment, HSA displays significantly different emission spectra, depending on the nature of the precursor and the presence of GLS. Entrapment into silica materials derived from TEOS, either with or without 17 mol % GLS, resulted in a blue shift in the emission spectra, consistent with HSA adopting a partially expanded conformation, which has been shown to be the first intermediate in the HSA unfolding pathway.[48] On the other hand, the emission spectra of HSA entrapped in both DGS- and DGS/GLS-derived materials showed maximum emission wavelengths that were essentially identical to that in solution, suggesting that HSA retains a more "nativelike" conformation in materials derived from DGS. The presence of a blue-shifted emission spectrum for HSA in TEOS-derived materials is likely due to the presence of ethanol, which is a byproduct of TEOS hydrolysis. The ethanol, which is present at levels of ca. 35% v/v,[55] is likely to induce partial unfolding of the entrapped HSA.[31] Interestingly, the presence of the covalently bound sugar does not appear to be able to overcome the ethanol-induced unfolding of HSA.

Dynamics of Entrapped HSA. Steady-state and time-resolved anisotropy studies were done to further examine the properties of HSA within the different silica materials. For these studies, HSA was site selectively labeled at Cys-34 with fluorescein-5-maleimide to produce HSA-F, rather than directly probing the anisotropy of Trp-214, to provide higher detection sensitivity and less interference from light scattering.

Figure 2 shows TRFA decays collected for HSA-F in solution and when entrapped into DGS/GLS-derived materials, and shows that the anisotropy decay of HSA-F in DGS/GLS-derived silica is significantly different from that in solution. Table 1 shows both steady-state and time-resolved anisotropy data for HSA-F as a function of aging time both in solution and in the different silica materials. Focusing first on the steady-state anisotropy data, it is clear that entrapment of HSA-F causes an increase in anisotropy, and hence a reduction in protein mobility, in all silica materials. The steady-state anisotropy values are highest in DGS-derived materials, followed by DGS/GLS, then TEOS, and finally TEOS/GLS. These data likely reflect the higher viscosity of

(54) Barrett, E. P.; Joyner, L. G. Halenda, P. H. *J. Am. Chem. Soc.* **1951**, *73*, 373.

(55) Flora, K. K.; Dabrowski, M. A.; Musson, S. P. Brennan, J. D. *Can. J. Chem.* **1999**, *77*, 1617−1625.

Table 1. Time-Resolved Fluorescence Anisotropy Decay Parameters for Free and Entrapped HSA as a Function of Aging Time

sample	ϕ_1,[a] ns	ϕ_2, ns	f_1[b]	f_2	r_0[c]	r[c]	g	r_{SS}[d]
solution	0.70	17.8	0.33	0.60	0.34	0.02	0.07	0.153
day 5 TEOS	2.12	7.75	0.32	0.19	0.33	0.16	0.49	0.221
day 15 TEOS	1.13	3.79	0.42	0.11	0.33	0.12	0.37	0.201
day 36 TEOS	0.97	5.53	0.35	0.07	0.24	0.14	0.58	0.194
day 5 G/TEOS	1.25	7.95	0.45	0.28	0.38	0.10	0.27	0.228
day 15 G/TEOS	0.79	4.89	0.35	0.06	0.35	0.20	0.59	0.225
day 36 G/TEOS	0.88	5.15	0.43	0.04	0.27	0.14	0.53	0.218
day 5 DGS	0.62	4.85	0.43	0.18	0.36	0.15	0.39	0.244
day 18 DGS	1.01	6.96	0.36	0.10	0.33	0.18	0.54	0.230
day 42 DGS	0.87	7.50	0.41	0.09	0.29	0.14	0.50	0.219
day 5 G/DGS	1.05	9.51	0.37	0.07	0.38	0.22	0.56	0.262
day 18 G/DGS	0.97	8.97	0.34	0.01	0.35	0.23	0.65	0.253
day 42 G/DGS	0.91	6.77	0.49	~0.00	0.31	0.16	0.51	0.247

[a] The typical error in rotational correlation times is ±2%. [b] The typical error in fractional contributions of anisotropy decay times is ±0.01. [c] Typical errors in r_0 values are ±0.01. [d] Typical errors in steady-state anisotropy values are ±0.005. All samples were tested in duplicate.

DGS-derived materials relative to TEOS-derived materials owing to the presence of high levels of entrapped glycerol, but may also reflect differences in protein conformation in TEOS-derived materials that lead to higher mobility in the region of Cys34. As aging proceeds, the steady-state anisotropy of entrapped HSA-F decreases, and thus mobility increases in the region of Cys-34, in all glasses. A similar decrease in anisotropy with time was also observed in solution (data not shown), suggesting that the protein undergoes partial unfolding in the region of Cys-34, making the bound fluorescein moiety more mobile as aging proceeds.

To gain further insight into the factors that influence the mobility of the protein, we examined the time-resolved decay of anisotropy of HSA-F. Considering the data in Table 1, it is apparent that entrapment leads to significant increases in the residual anisotropy for HSA-F in all materials. Furthermore, the shorter correlation time, corresponding to local motion of the bound probe, increases in magnitude and proportion, while the longer rotational correlation time, corresponding to global and/or segmental motion, appears to *decrease*, in both magnitude and proportion, upon entrapment. These data agree with previous TRFA data of Trp-214 in HSA entrapped into TEOS-derived materials,[31] and can be rationalized as follows: in solution, the high proportion of the long decay time of HSA-F, coupled with the lack of a substantial residual anisotropy value, suggests that this value is a convolution of both global and segmental rotational reorientation times in the region of Cys-34. This is supported by the fact the longer rotational reorientation time of ca. 18 ns is less than half the value of the reported global rotational reorientation time of HSA (40 ns).[56] Upon entrapment, the loss of global motion, as indicated by the high residual anisotropy, results in only segmental motion contributing to the longer decay time. As a result, both the magnitude of the decay time and the overall proportion of this decay time decrease, since global motion no longer contributes to the value of f_2. Overall, this indicates that upon entrapment the HSA adsorbs to the surface of the gel, likely through a region other than domain I, given that this domain retains significant segmental motion.

As shown in Table 1, the decay of anisotropy for entrapped HSA-F is dependent on both the nature of the material and the length of aging. The loss in motion upon entrapment is most dramatic in DGS-derived materials, where the contribution from segmental motion is only 7% in DGS/GLS-derived materials and 18% in DGS-derived materials, versus ca. 20% and 28% for TEOS- and TEOS/GLS-derived materials, respectively. This is consistent with the findings obtained from the steady-state anisotropy data. Aging of materials also caused significant changes in protein dynamics. In all cases, aging caused a significant decrease in f_2 (loss of segmental motion) with a corresponding increase in f_1, consistent with increased local motion in the vicinity of Cys-34. There was also an increase in residual anisotropy with aging, consistent with increased restriction of overall protein motion. Taken together, these data are indicative of surface adsorption and unfolding of the protein in the local region of Cys-34. A particularly noteworthy change in anisotropy with aging was displayed by the DGS/GLS sample, where there was essentially complete loss of both global and segmental motion as aging proceeded. A similar but much less pronounced decrease in segmental motion was observed for TEOS/GLS samples, where segmental motion contributed less than 5% to the total motion after 36 days of aging.

The retention of partial segmental motion within domain I for HSA entrapped in TEOS- and DGS-derived materials indicates that the protein likely adsorbs in a different orientation, likely via electrostatic interactions, resulting in exposure of domain I to the pore solvent in such materials. This is consistent with previous results from Bright et al.,[6] who also observed retention of mobility for domain I of entrapped HSA labeled with acrylodan at Cys-34. Given that our previous studies of HSA dynamics in TEOS using Trp-214 demonstrated significant mobility for domain II of the protein, and given that domains I and II of HSA have a net negative charge,[57] which would be expected to reduce interactions with anionic silica materials, it is highly likely that in undoped silica the protein adsorbs through domain III. The complete loss of global motion in undoped silica is consistent with the results obtained by Friedman and co-workers for myoglobin[7] and by Bright et al. for the anti-dansyl antibody,[8] which showed these entrapped proteins

(56) Yguerabide, J.; Epstein, H. F.; Stryer, L. *J. Mol. Biol.* **1970**, *51*, 573−590.

(57) (a) Carter, D. C.; Ho, J. X. *Adv. Protein Chem.* **1994**, *45*, 153−203. (b) Brown, J. R. In *Albumin Structure, Function and Uses*; Rosenoer, V. M., Oratz, M., Rothschild, M. A., Eds.; Pergamon: Oxford, 1977; pp 27−51.

to be essentially immobile after aging of TEOS-derived glasses. These latter results have been interpreted in terms of electrostatic interactions between the protein and silicate at neutral pH,[7,58] or in terms of templating of the silicate around a relatively rigid protein,[8] leading to little or no segmental motion and to very slow tumbling within the glass owing to the higher microviscosity of the internal solvent.

In the presence of GLS, it is noted that the dynamics of domain I become restricted with time, and in the case of DGS/GLS become almost completely arrested. This result shows that in GLS-modified glasses adsorption of the protein through domain I is likely. The presence of the GLS would be expected to cause a reduction in the number of silanolate sites available for electrostatic binding to the protein, but on the other hand would provide a large number of sites capable of hydrogen-bonding to the protein. The reduction in HSA dynamics is therefore likely to be due to strong hydrogen bonding between various uncharged amino acids in the protein and the covalently bound sugar moieties. These results suggest that the use of sugar additives may provide a method to tune the dynamics of entrapped proteins, which may aid in stabilizing the protein against denaturation, as shown below.

Thermal Stability Studies of Entrapped HSA. Figure 3 shows the changes in the normalized fluorescence intensity and emission wavelength of Trp-214 for free and entrapped HSA as a function of temperature. Trp-214 was chosen as the probe for this study owing to the significant change in Trp fluorescence intensity as a function of protein unfolding,[48] and to allow direct comparisons to previous thermal stability studies of HSA in solution[48] and in TEOS-derived materials.[31] As shown in Figure 3A, the entrapment of HSA leads to a significant increase in the unfolding temperature of the protein, regardless of the material composition. This effect has been reported previously in several papers,[4,59−61] and is thought to be the result of an increased entropy of unfolding owing to molecular confinement.[44,45] The electrostatics in the vicinity of the entrapped protein may also play a role in the stabilization, as high levels of anions have been observed to stabilize HSA in solution.[62]

To further examine the effects of the precursors and covalently tethered sugar on the unfolding of HSA, the maximum emission wavelength of the protein was examined as a function of temperature. As shown in Figure 3B, materials containing TEOS initially show a red shift in emission wavelength with temperature, but in the case of unmodified TEOS there is a shift back to shorter wavelengths at approximately 60 °C, which corresponds to the point where the intensity is reduced by ∼40% relative to that of the native protein. This shift toward short wavelengths suggests that some kind of rearrangement or perhaps some aggregation

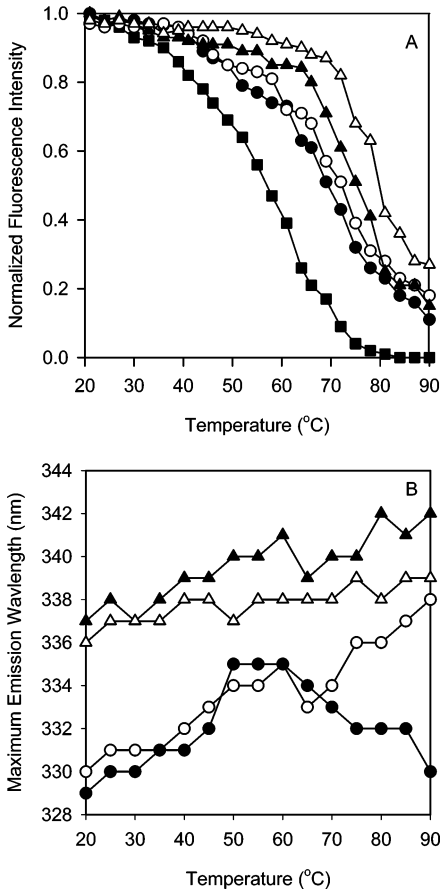

Figure 3. (A) Changes in intensity and (B) changes in emission wavelength during thermal unfolding for free HSA and entrapped HSA after 15 days of aging in various materials: (■) solution; (●) TEOS; (○) TEOS/GLS; (▲) DGS; (△) DGS/GLS.

occurs in the vicinity of Trp-214 during unfolding in TEOS. HSA in materials derived from TEOS/GLS showed a large red shift in emission wavelength, which continued as the temperature was increased to 90 °C. The final emission wavelength was on the order of 338 nm, which is consistent with partial unfolding of the protein in the region of Trp-214. HSA within both DGS and DGS/GLS showed small red shifts in emission wavelength to 343 nm (DGS) and 339 nm (DGS/GLS), consistent with partial unfolding of HSA. The smaller red shift for DGS/GLS suggests a lower degree of unfolding, consistent with the intensity data, and confirms that GLS imparts additional thermal stability to entrapped HSA.

In comparing the thermal stability of HSA in the different materials, it is clear that the stability of HSA entrapped in DGS/GLS-based materials is highest, followed by materials derived from DGS, TEOS/GLS, and TEOS. The data show that HSA in either DGS or DGS/GLS materials is unable to unfold completely, on the basis of the smaller overall changes in intensity and emission wavelength relative to those of the solution. These changes in thermal stability highlight the effects of the precursor and additive, and show that, in cases where a nonbiocompatible precursor, such as TEOS, is used, the addition of protein-stabilizing additives such as GLS has little effect on improving protein stability. The use of a biocompatible precursor, such as DGS, resulted in a significant improvement in thermal stability relative to that of either TEOS or TEOS/GLS, and the addition of GLS resulted in

(58) (a) Chen, Q.; Kenausis, G. L.; Heller, A. *J. Am. Chem. Soc.* **1998**, *120*, 4582−4585. (b) Heller, J.; Heller, A. *J. Am. Chem. Soc.* **1998**, *120*, 4586−4590.
(59) Flora, K. K.; Brennan, J. D. *Anal. Chem.* **1998**, *70*, 4505−4513.
(60) Zheng, L.; Flora, K. K.; Brennan, J. D. *Chem. Mater.* **1998**, *10*, 3974−3983.
(61) Eggers, D. K.; Valentine, J. S. *Protein Sci.* **2001**, *10*, 250−261.
(62) Muzammil, S.; Kuman, Y.; Tayyab, S. *Proteins* **2000**, *40*, 29−38.

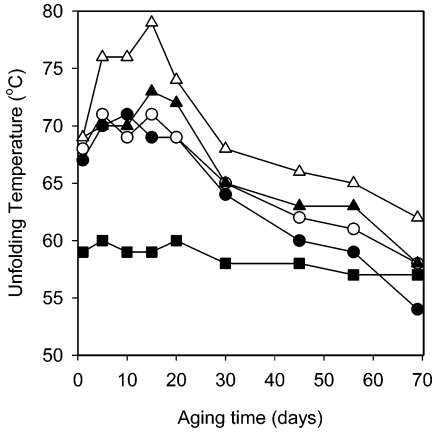

Figure 4. Changes in unfolding temperature of HSA as a function of aging time in different sol−gel-derived materials: (■) solution; (●) TEOS; (○) TEOS/GLS; (▲) DGS; (△) DGS/GLS.

further improvements in protein stability. These results suggest that use of a biocompatible precursor is a key requirement for improving protein stability, with additives imparting a further benefit only when such precursors are used. Use of an alcohol-generating precursor likely causes the potential benefits of the covalently coupled sugar to be largely negated, in agreement with previous studies from our group, which have shown improved activity for enzymes entrapped in DGS and DGS/GLS materials, but not in TEOS/GLS materials.[46,47]

It is interesting to compare the thermal stability data to the dynamics of entrapped HSA in the different materials. As noted above, the dynamics of HSA after 15 days of aging show the greatest mobility in TEOS-derived materials, somewhat lower mobility in TEOS/GLS and DGS, and the lowest mobility in DGS/GLS. Given that one of the key factors that influences thermal stability is the ability of the protein to adopt an unfolded conformation, one should expect that proteins with decreased mobility would have increased thermal stability. This general trend is observed in this work, and highlights one of the potentially important roles of GLS in maintaining the activity of proteins after entrapment. While this is important, it must also be remembered that the precursor will determine the stability of the protein during and immediately after entrapment, and it is expected, on the basis of the results above, that this factor must also be optimized to maximize protein activity.

Figure 4 shows the unfolding temperatures calculated for free and entrapped HSA samples as a function of sample aging. As aging proceeds, the unfolding temperature first increases and then decreases, with the greatest increase in unfolding temperature being observed for the DGS/GLS sample. The apparent increase in the thermal unfolding temperature of the entrapped proteins at early aging times, coupled with the spectroscopic evidence for incomplete unfolding, is consistent with previous reports,[4,31,60] and suggests that the internal environment of the sol−gel-derived glass is able to restrict large-scale conformational changes in the protein. This effect is most pronounced in DGS and DGS/GLS materials, in which HSA starts from a native conformation. The results for HSA in TEOS-derived materials are more difficult to interpret, as in these materials the protein is likely to be partially unfolded prior to thermal

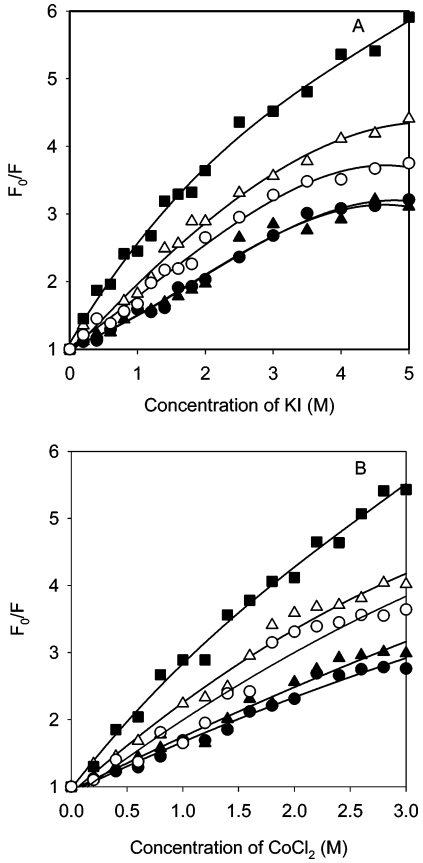

Figure 5. Accessibility of entrapped HSA to (A) the anionic quencher KI and (B) the cationic fluorescence quencher $CoCl_2$ in solution and in sol−gel-derived materials after 15 days of aging: (■) solution; (●) TEOS; (○) TEOS/GLS; (▲) DGS; (△) DGS/GLS. The lines are polynomial fits that are provided to highlight the curvature in the quenching plots.

denaturation studies. Hence, the unfolding temperatures are likely only approximate indicators of overall stability, as they do not reflect unfolding from a fully native conformation to a fully unfolded state, as is the case in solution. Furthermore, our results suggest that the increased unfolding temperatures are transient, as aging causes the unfolding temperature of the entrapped protein to eventually decrease to a value equal to or lower than that of the protein in solution. Overall, the results show that entrapment of the protein will not necessarily lead to an improvement in long-term thermal stability, at least under the storage conditions employed in this study. Even so, the results show that the sugar-doped materials maintain the thermal stability of HSA to a greater extent than do undoped materials, particularly for DGS materials.

Accessibility of Entrapped HSA. Figure 5 shows Stern−Volmer (SV) quenching data for free and entrapped HSA upon exposure to both anionic (I^-) and cationic (Co^{2+}) quenchers, which were selected to allow us to examine the effects of electrostatic interactions on protein accessibility to external analytes. The Stern−Volmer plots for HSA in solution are linear, indicative of pure dynamic quenching of HSA by both quenchers, with no effects from either static quenching or inaccessibility of the bound fluorescein probe to either quencher. However, in the case of entrapped HSA, the majority of Stern−Volmer curves show significant downward curvature, indicative of a fraction of protein that is not able to be quenched by externally added I^- or Co^{2+}. The initial slopes of the SV curves for entrapped HSA are

Table 2. Accessibility of Free and Entrapped HSA to Anionic and Cationic Quenchers[a,b]

sample	K_{sv}, M^{-1}	k_q, $10^8\ M^{-1}\ s^{-1}$	τ_0, ns	r^2	intercept	f_i
KI Quenching						
solution	1.79	4.40	4.07	0.95	1.02	0
TEOS, 5 days	0.79	2.05	3.85	0.97	0.96	0.20
TEOS, 35 days	0.65	1.75	3.71	0.95	0.97	0.35
GLS/TEOS, 5 days	1.01	2.60	3.88	0.96	1.09	0.05
GLS/TEOS, 35 days	0.87	2.17	4.01	0.97	0.99	0.15
DGS, 5 days	0.83	2.10	4.15	0.95	0.97	0.05
DGS, 37 days	0.72	1.84	3.92	0.95	0.95	0.25
GLS/DGS, 5 days	1.02	2.49	4.10	0.96	1.08	0.05
GLS/DGS, 37 days	1.21	3.02	4.02	0.94	1.06	0.15
Co^{2+} Quenching						
solution	2.05	5.04	4.07	0.96	0.97	0
TEOS, 5 days	0.89	2.31	3.85	0.95	1.10	0.15
TEOS, 38 days	0.61	1.64	3.71	0.95	0.99	0.35
GLS/TEOS, 5 days	0.85	2.19	3.88	0.98	0.96	0.05
GLS/TEOS, 38 days	0.74	1.85	4.01	0.97	0.98	0.20
DGS, 7 days	0.98	2.36	4.15	0.99	0.95	0.10
DGS, 35 days	0.71	1.81	3.92	0.96	1.06	0.20
GLS/DGS, 7 days	1.43	3.49	4.10	0.98	0.99	0.05
GLS/DGS, 35 days	1.27	3.16	4.02	0.96	0.96	0.15

[a] Data were obtained by fitting the quenching data to eq 2. [b] Typical errors in K_{SV} and k_q are 5% (RSD), typical errors in τ_0 are 2% (RSD), and typical errors in f_i are ±0.05. All samples were tested in duplicate.

also lower than those obtained in solution, indicative of a lower degree of quenching for the accessible fraction of HSA. Table 2 shows the Stern−Volmer quenching data obtained by fitting the quenching curves to eq 2 for free and entrapped HSA in the presence of each quencher. Several points merit further attention. First, the k_q values drop for HSA upon entrapment into any silica material, regardless of the quencher, indicative of restricted diffusion of quenchers through the matrix. Second, the k_q values tend to drop as aging proceeds, consistent with increased syneresis and expected decreases in pore size with aging for all materials. Third, all entrapped proteins show at least some degree of inaccessibility to quenchers, with the fraction of inaccessible protein increasing with aging. Fourth, the degree of quenching and the fraction of accessible protein depend to a large degree on the material composition, with the k_q values and fractional accessibility being greatest in materials containing GLS, followed by DGS-derived materials and finally TEOS-derived materials. Last, quenching does not appear to depend on the charge of the quencher, with accessibility to both anionic and cationic quenchers being essentially equivalent in all materials tested.

Given that the unmodified silicate matrix is negatively charged at the experimental pH of 7.2, it is likely the anionic quencher KI was unable to penetrate into all regions of the matrix. Conversely, the cationic quencher $CoCl_2$ may be adsorbed to the walls of the silicate matrix to some extent and therefore may be unable to penetrate entirely to the interior of the silicate matrix. Materials with covalently bound sugars would be expected to have significantly lower levels of anionic sites available for interaction with the charged quenchers, on the basis of previous studies of binding of charged fluorophores to GLS-modified Ludox materials.[49] Such materials would also have a lower cross-link density, which may provide for larger overall pores. This would reduce electrostatic interactions between the analytes and the silica surface and increase the rate of diffusion, improving accessibility.

Table 3. Shrinkage and BET Data for Different Sol−Gel-Derived Materials[a]

precursor	% (v/v) shrinkage[b]	multipoint BET area,[c] m^2/g	pore volume, cm^3/g	average pore radius, nm
TEOS	70	615	0.49	1.8
GLS/TEOS (1:5)	43	55	0.33	2.0
DGS	54	591	0.49	2.2
GLS/DGS (1:5)	13	33	0.19	2.5

[a] All data were obtained by analyzing the desorption branch of the isotherm using the BJH equation. [b] Volume shrinkage values are obtained from samples after 60 days of aging in air at 4 °C. [c] Typical errors are 5% RSD for surface area, 10% RSD for pore volume, and 5% RSD for pore radius. All samples were tested in duplicate.

Accessibility is also likely to be dependent on changes in pore morphology for the various materials. As shown in Table 3, the pore size of DGS- and DGS/GLS-derived materials is somewhat larger than that of TEOS or TEOS/GLS materials, and the degree of shrinkage, which we assume correlates to the degree of pore collapse, is much lower for DGS- and DGS/GLS-derived materials. Both of these factors are likely to improve the rate of diffusion of the analytes through the matrix, consistent with the increased k_q values and accessibility for both of the quenchers in DGS and DGS/GLS materials relative to TEOS-based materials. The improved accessibility is likely to be a significant factor in the increased activity of entrapped enzymes noted elsewhere,[47] since this would increase the rate of delivery of the substrate.

Ligand-Binding Studies. While investigations of conformation, dynamics, and thermal stability provide information regarding how entrapment affects protein structure and mobility, the most important parameter that determines the success of a particular host material for entrapment is the degree of ligand-binding capacity retained by the entrapped protein. For this reason, the ability of entrapped HSA to bind to the model fluorescent ligand salicylate was assessed for all materials studied. Figure 6A shows binding isotherms obtained from free and entrapped HSA after 2 days of aging. The data show that the degree of ligand binding decreases relative to that in solution for HSA entrapped in all materials, as indicated by the smaller decrease in Trp fluorescence intensity. Examination of the binding isotherms shows that the dissociation constants (K_d), estimated using the concentration of ligand that gives half of the maximum intensity change in the isotherms, are relatively similar in all cases. The value in solution is ∼6 μM, while the values for entrapped HSA are all approximately 7 μM, indicating that entrapment does not alter the dissociation constants. The lower changes in intensity upon addition of salicylate are therefore attributed to the presence of a fraction of denatured and/or inaccessible protein that is unable to bind to the ligand. The latter is consistent with the lower accessibility of the protein to the anionic quencher I^-.

Figure 6B shows the relative degree of ligand binding as a function of aging for free and entrapped HSA. It is clear that the entrapment of HSA results in an immediate decrease in ligand-binding ability relative to that in solution, regardless of the material. However, the greatest retention of activity is observed for the DGS/GLS system, which retained ∼70% of the solution binding activity. The other materials retained 55−60% activity immediately after entrapment. Given that

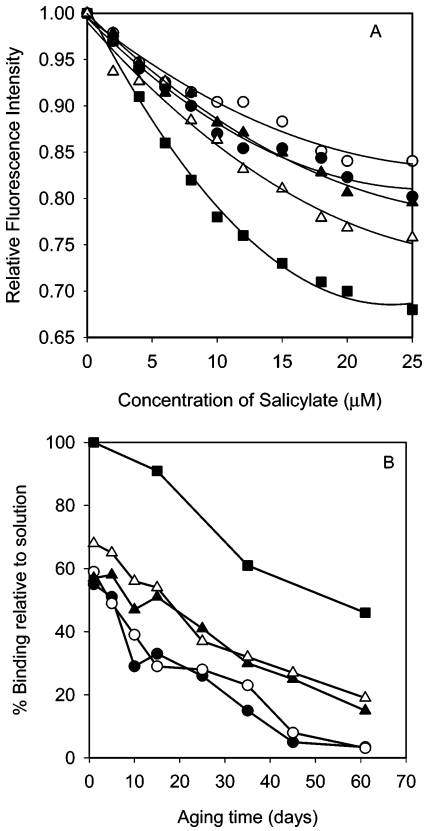

Figure 6. (A) Binding curves for HSA in solution and when entrapped in different silica materials after 2 days of aging and (B) percentage of ligand binding retained vs solution at a salicylate:protein molar ratio of 1.75 as a function of aging time in different materials: (■) solution; (●) TEOS; (○) TEOS/GLS; (▲) DGS; (△) DGS/GLS. The protein concentration is 10 μM. The lines are polynomial fits meant to guide the eye.

the accessibility to I^- was generally >90% for freshly prepared samples, it is likely that accessibility is not the major factor contributing to the loss in activity. Rather, it is likely that there is a fraction of denatured protein present after entrapment that causes activity to be reduced relative to that in solution.

As aging proceeds, both free and entrapped HSA show large decreases in ligand-binding activity, with free HSA showing 55% of the initial activity after 45 days of aging, and entrapped samples showing between 10% (TEOS and TEOS/GLS) and 30% (DGS and DGS/GLS) activity, relative to the initial activity of HSA in solution. The losses in activity are likely due to a combination of long-term denaturation of HSA and decreases in analyte accessibility. The key finding from this study was that the loss of activity was dependent primarily on the nature of the precursor used (TEOS vs DGS), with little or no improvement in binding activity imparted by GLS. This result is likely to be protein specific, particularly given our recent findings for various enzymes in different sol−gel-derived materials. For example, enzymes such as urease and luciferase show no activity in TEOS, TEOS/GLS, or DGS materials, and are active only when relatively high levels of GLS are present in DGS-derived materials. On the other hand, factor Xa shows a major improvement in activity in DGS relative to TEOS, but no additional increase in activity when GLS is present in DGS. In the case of HSA, it appears that the most important constituent of the sol−gel material is the biocompatible precursor, although GLS does impart small additional improvements in activity.

Conclusions

The properties of entrapped HSA, including conformation, dynamics, accessibility to external analytes, thermal stability, long-term stability, and degree of ligand binding, depend on both the nature of the silica precursor and the addition of covalently tethered sugars; in the case of HSA the most important of these factors is the nature of the silica precursor. In general, addition of GLS to a biocompatible silica material formed from DGS led to improvements in protein activity and stability, while addition of the covalently bound sugar to TEOS-derived materials imparted minimal improvements in protein performance. These results highlight the importance of alcohol-free processing.

A key aspect of the effect of GLS on protein behavior is the significant decrease in protein mobility in materials that contain this additive. This factor may be partially responsible for the improved thermodynamic stability of HSA, likely owing to restricted conformational motion. GLS may also lead to reduced electrostatic surface repulsion of analytes, and better overall protein accessibility to charged analytes. The results therefore suggest that tuning the level and nature of the sugar within the matrix may provide a mechanism to manipulate protein dynamics and accessibility, and thus optimize the activity and stability of the entrapped protein.

Acknowledgment. We thank the Natural Sciences and Engineering Research Council of Canada, MDS-Sciex, the Ontario Ministry of Energy, Science and Technology, the Canadian Foundation for Innovation, and the Ontario Innovation Trust for financial support of this work. M.A.B. gratefully acknowledges the Canada Council for the Arts for a Killam Fellowship. J.D.B. holds the Canada Research Chair in Bioanalytical Chemistry.

CM048166C